Optimizing the individual design of revision hip implants – evaluating the effects for bone and stem using patient-specific finite element models

David Scherb[1,*], Maria Helena Barbosa[1], Harald Völkl[1], Christopher Fleischmann[2], Marcel Betsch[3], Stefan Sesselmann[4], Sandro Wartzack[1], Jörg Miehling[1]

[1] Engineering Design, Friedrich-Alexander-Universität Erlangen-Nürnberg (FAU), Martensstr. 9, 91058 Erlangen, Germany
[2] Institut für Medizintechnik, Technical University of Applied Sciences Amberg-Weiden, Hetzenrichter Weg 15, 92637 Weiden, Germany.
[3] Department of Trauma and Orthopedic Surgery, University Hospital Erlangen, Friedrich-Alexander-Universität Erlangen-Nürnberg (FAU), Erlangen, Germany
[4] Technical University of Applied Sciences Würzburg-Schweinfurt, Münzstr. 12, 97070 Würzburg, Germany

** Korrespondierender Autor:*
David Scherb
Martensstraße 9
91058 Erlangen
☎ *+49911 5302-96618*
✉ *scherb@mfk.fau.de*

Abstract

Patient-specific musculoskeletal models (MSM) can improve the selection and positioning of revision total hip arthroplasty (THA) during preoperative planning. By accounting for muscle weakening due to surgical procedures, MSMs provide more accurate load data for finite element models in preclinical testing. This paper presents a preclinical study using finite element analysis (FEA) to investigate the effects of changes in hip parameters – femoral neck angle, antetorsion and femoral offset – on implant longevity after revision. 57 proximal femur CAD models, based on MRI scans of a patient, were used to create femoral implants with unique parameter combinations. FEA simulations of stair climbing, which accounted for reaction forces of the hip joint, showed that all parameter changes affected the stress distributions, with the increase in antetorsion having the strongest effects on bone-implant interface stresses.

Keywords

Patient-specific musculoskeletal models, Revision total hip arthroplasty, Cement-in-cement technique, Finite element models, Parameter study

 | DOI: 10.35199/dfx2024.02

1. Introduction

The number of total hip replacements (THR) performed in Germany each year is steadily increasing [1, 2]. The number of revision procedures, i.e., the replacement of an implanted hip with a new implant, is also increasing accordingly. The main cause for subsequent revisions is implant loosening [1]. Pre-clinical tests are crucial in predicting the durability of femoral stems' fixation because this failure mode often results from mechanical complications [3]. Mainly, Finite Element (FE) simulations are conducted, in order to analyse the debonding and failure of the interface, to simulate the occurring damage in bone and implant or to determine the longterm durability of the implant [4–6]. Due to functional purposes that the final implant configuration should be well adjusted to the patient's biomechanics, a preoperative planning process based on medical imaging is carried out with the aim of determining the optimal setup of the prosthesis, i.e., the most suitable combination of hip implant parameters (e.g., neck-shaft angle (NSA), (femoral) offset or antetorsion angle (AT)) for the patient prior to every (revision) THR. Nevertheless, there is a high probability of muscular dysfunction, particularly after a revision THR, which manifests itself in a pathological gait pattern, such as the Trendelenburg gait [7]. The reason for this is an implant configuration that is not optimally adjusted to the weakened muscular siuation of the patient [8], which leads to protracted and, in the worst case, incomplete rehabilitation. The non-optimal implant placement is due to the shortcomings in the preoperative planning process, which mainly focuses on the bony structures and the fit of the implant for them and does not sufficiently consider the effects on the muscular parts. Therefore, a new, comprehensive approach to the preoperative planning of revision THR (or, more precisely, to the identification of the design of the revision implant) would be of great benefit in terms of patient needs. The integration of preoperative simulations could significantly improve the postoperative results of revision THA. Musculoskeletal human models (MHMs) can be used to investigate the effects of various changes in hip parameters on the muscular side [9, 10]. However, the optimal implant setup always results as a balance of considering effects between muscular and bony structures or implant. In order to consider the effects of the various selectable parameters for revision implants on the anchoring of the implant in the bone, a FE analysis should therefore be carried out in addition to musculoskeletal human simulation. These results can then be used to develop a comprehensive simulative approach to determine the optimal revision hip implant configuration for specific patients. The research question in this contribution is: How do the adjustable parameters for hip revision implants influence the stresses occurring in a patient's bone and implant structure in the case of a revision THR?

2. Materials and Methods

For a revision THR, the cement-in-cement technique has been reported to be employed in a considerable proportion of the number of cases where cemented components were revised [11]. This technique consists of recementing the prosthetic component into the well-fixed mantle to prevent the complications associated with the removal of an intact cement mantle during the revision THR [12]. When used for various clinical purposes (e.g., replace a broken stem in an intact mantle, increase the acetabular exposure), as long as the old cement mantle remains intact at least in the two more distal thirds of the implant, it is less time consuming and has highly satisfactory postoperative outcomes [11, 13]. Thus, in this study the cement-in-cement technique is used for evaluation.

2.1. Finite Element models

The FE models were set up using Ansys® Mechanical software. Based on an MRI scan of a subject, the left femur was extracted to a volumentric model (STL file) using a process called

“Segmentation” [14]. In this volumetric model, the trabecular (soft part of the bone) and cortical bone (hard part of the bone) was modelled (see Figure 1A). The challenge in this task is the modelling of the proportion of the trabecular bone from the whole bone. The trabecular bone was designed by scaling and remodeling the cortical geometry until obtaining a smaller solid, then used to extract the interior cortical volumes. A study conducted by Dorr et al. [15] was used as a reference for setting up this cancellous bone model. The subject’s femoral cortex was scaled until the medial-lateral cortical index would fall between the mean values determined in the study. The medial-lateral cortical index is given by the difference between the diaphyseal diameter and intramedullary canal diameter divided by the diaphyseal diameter, in a section located 10 cm below the mid lesser trochanter (see Figure 1B). The final 3D femoral geometry used in this work has a medial-lateral cortical index equal to 0.54.

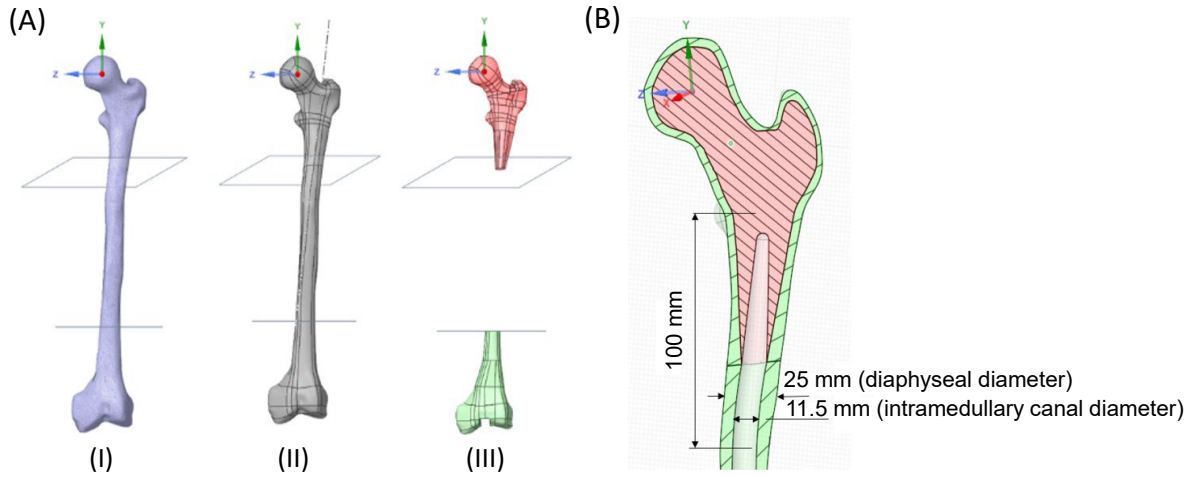

Figure 1: (A) Subject’s femur model geometries. (I) STL file of the subject’s cortical bone generated from MRI image. (II) CAD geometry of the cortical bone, displaying the proximal femur longitudinal axis. (III) Proximal and distal trabecular bone geometries, (B) Section view with indications of the dimensions used for the medio-lateral cortical index.

The cement mantles were assumed to consist of Polymethylmethacrylat (PMMA) and were built in two steps. First, single mantles of primary THR were designed with a minimum thickness of 2-5 mm to follow the recommendation for optimum mantles thickness from Ebramzadeh et al. [16]. The maximum thicknesses didn’t exceed 5 mm in any of the models. Afterwards, new-cement mantles were designed around the stems, all of them with minimum mantle thickness of 1 mm, proximally, and maximum thickness of 3.5 mm in more distal regions. As revision THR implants, 125 mm length Exeter stems were used in this study due to progressive increase in the use of short-stems in elective THAs in Germany [1] and the satisfactory outcomes of cement-in-cement femoral revision THR with this stems pointed out in recent studies [17, 18]. The implants were positioned in the bone model aligned to the proximal femur shaft axis. The interface contacts were set as perfectly bonded. The chosen material parameters of the different parts of the model are based on different studies available in literature [5, 19–22], which are summarized in Table 1. Isotropic materials were considered for the characterization of the cement mantles, the femoral stem, and the prosthetic head. All geometries were meshed using quadratic tetrahedral elements. The mesh elements’ size and, therefore, the number of mesh elements was defined after convergency studies based on the von Mises stresses for the implant. In order to make the stress distributions in the stem-cement interface less sensitive to the fraction of nodes per unit area, a finer discretization was ensured by locally defining the edge size of the elements adjacent to the interface as 1.65 mm.

Table 1: Chosen material properties for several parts of the FE model based on [5, 19–22]

Elastic properties			
Model part	Poisson's ratio	Elastic modulus	Shear modulus
Femoral Cortex	ν_{xy} = 0.58 $\nu_{xz} = \nu_{yz}$ = 0.31	$E_{xx} = E_{yy}$ = 17 Gpa E_{zz} = 11.5 GPa	$G_{yz} = G_{zx}$ = 3.28 Gpa G_{xy} = 3.63 GPa
Trabecular bone	ν_{xy} = 0.093 ν_{xz} = 0.149 ν_{yz} = 0.098	E_{xx} = 373 MPa E_{yy} = 203 MPa E_{zz} = 340 MPa	G_{yz} = 24 MPa G_{xy} = 22 MPa G_{xz} = 24 MPa
Old PMMA	v = 0.3	E = 2.08 GPa	
New PMMA	v = 0.3	E = 2.12 GPa	
Stem	v = 0.3	E = 200 GPa	
Prosthetic head	v = 0.23	E = 380 GPa	

2.2. Revision hip implant variation

As previously mentioned, the main varying parameters in hip revision implants to adjust the prosthesis towards the patients are the NSA, offset and AT. Based on the previous study by Scherb et al. [9] investigating the influence of the adjustable parameters for the muscles via musculoskeletal simulation, the parameter combinations were chosen similar. Five NSAs - 110°, 117°, 120°, 125°, 150° - four offsets – 30, 35, 40, 50 mm – and 3 ATs – 8°, 18°, 38° - were selected as parameter values. For each parameter combination, an individual hip revision implant model was created, an example is shown in Figure 2. As decribed in section 2.1, each created implant model was inserted in the modelled bone aligning the stem shaft axis and proximal femur shaft axis and assigning the material parameters (Table 1). Thus, 57 FE models with individual virtually implanted hip revision implant into the patient femur resulted.

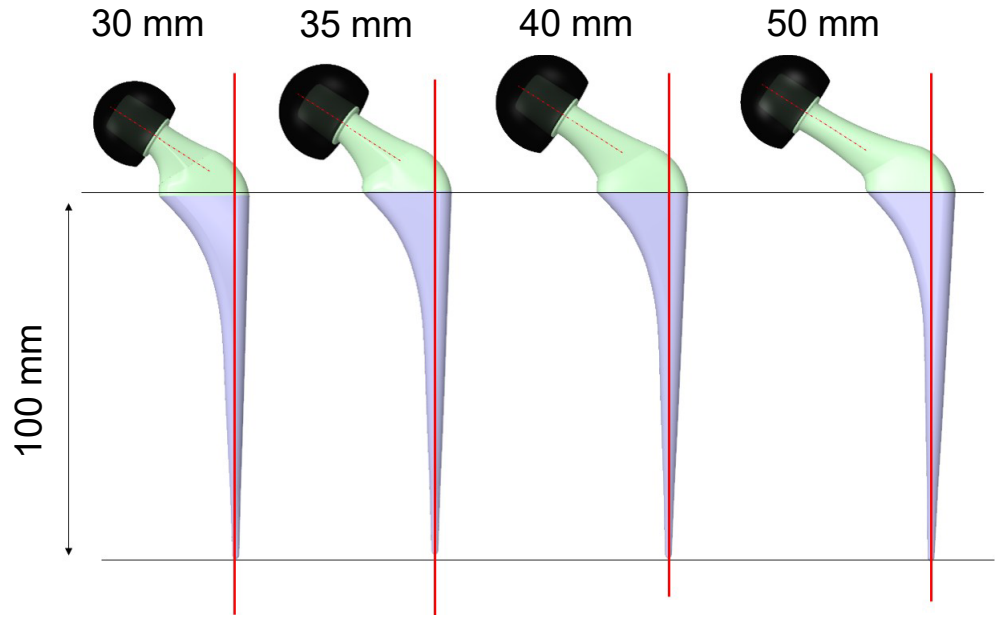

Figure 2: Stem models with 125° NSA and varying offset. The dashed red lines are axial to the stems' necks and form a 125º NSA with the solid red lines. The solid red lines are the stem's shaft axes which were aligned to the proximal femur shaft axis.

2.3. Load Analysis

Lastly, the external applied force to the implants has to be inserted for the FE analysis. These were determined using musculoskeletal simulation in OpenSim [23] (Figure 3). The same MHM from Scherb et al. [9], which is characterized by an patient-specific modelled anatomy and muscles in the hip area [24], was used. The real subject for this model was recorded in a motion capture laboratory performing different activities of daily living (e.g, walking, standing up from a chair, stair climbing etc.). After transferring the motion data to the MHM, it was observed the highest hip joint contact forces occurred during the stair climbing. Thus, under the assumption that the highest stem-cement-bone interface stresses and accordingly the highest load for the implant and bone would occur with the highest hip joint contact forces, the stair climbing was chosen for further analysis.

The different parameter combinations of NSA, offset and AT of the FE models (57 in total) were remodelled in the MHM and under consideration of the captured stair climbing motion, the resulting hip joint contact force was simulated. The highest occurring force in this simulation was extracted and applied to the corresponding FE model, performing a static FE analysis. In the FE analysis, the occurring stresses in the stem-cement interface and the stress distribution in the cement mantles are investigated.

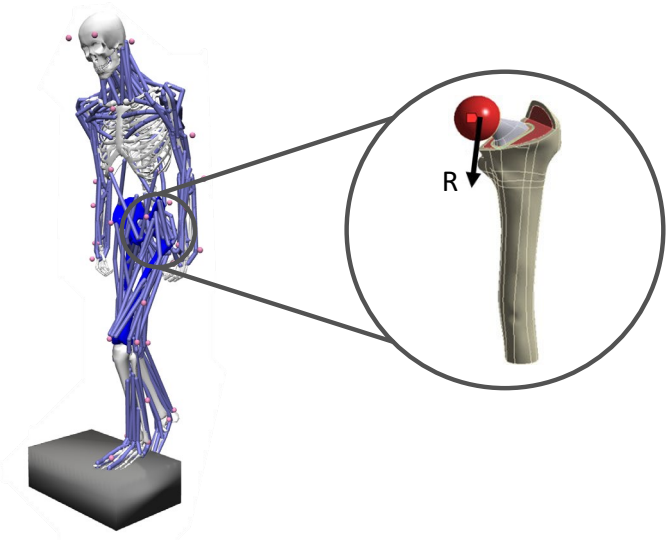

Figure 3: Musculoskeletal simulation of stair climbing and application of resulting hip joint contact force on hip revision implanted FE models

3. Results

3.1. Stem-cement interfacial damage

For evaluation of the stem-cement interfacial damage, a parameter called stem-cement interfacial damage extent is used. The stem-cement interfacial damage extent is defined as the percentage of nodes at the interface where the calculated averaged tensile and shear stresses exceed mean strength values for tensile stress (2.81 MPa) and shear stress (1.39 MPa) [6]. For the models with AT angles 8° and 18°, none of the stress values found were superior to the interface strengths. Regarding the models with 38° AT, the quantified interface damage due to both tensile and shear stresses varied similarly when only one of the hip parameters (NSA or offset) is modified. Observing the results for models with the same offset, both the percentages of shear and tensile failure decrease with the increase in the NSA until reaching 125°, except for tensile failure in the models with 50 mm offsets (see Figure 4a). The increase

in the NSA from 125° up to 150° results in the increase of the damage extension in the models with 30 mm offsets. When studying the results of models with the same NSA, as illustrated in Figure 4b, it can be noticed that as the offset increases, until it is equal to 40 mm, the percent damage decreases, except in the tensile damage case for models with a 50 mm offset. From the 40mm to the 50mm offset, the percentage of interface failure increases. Furthermore, the damage extent due to shear stresses is more expressive than the damage due to tensile stresses. The peak stresses reach the highest values in the models with 38° AT, and, between the 8° and 18° models.

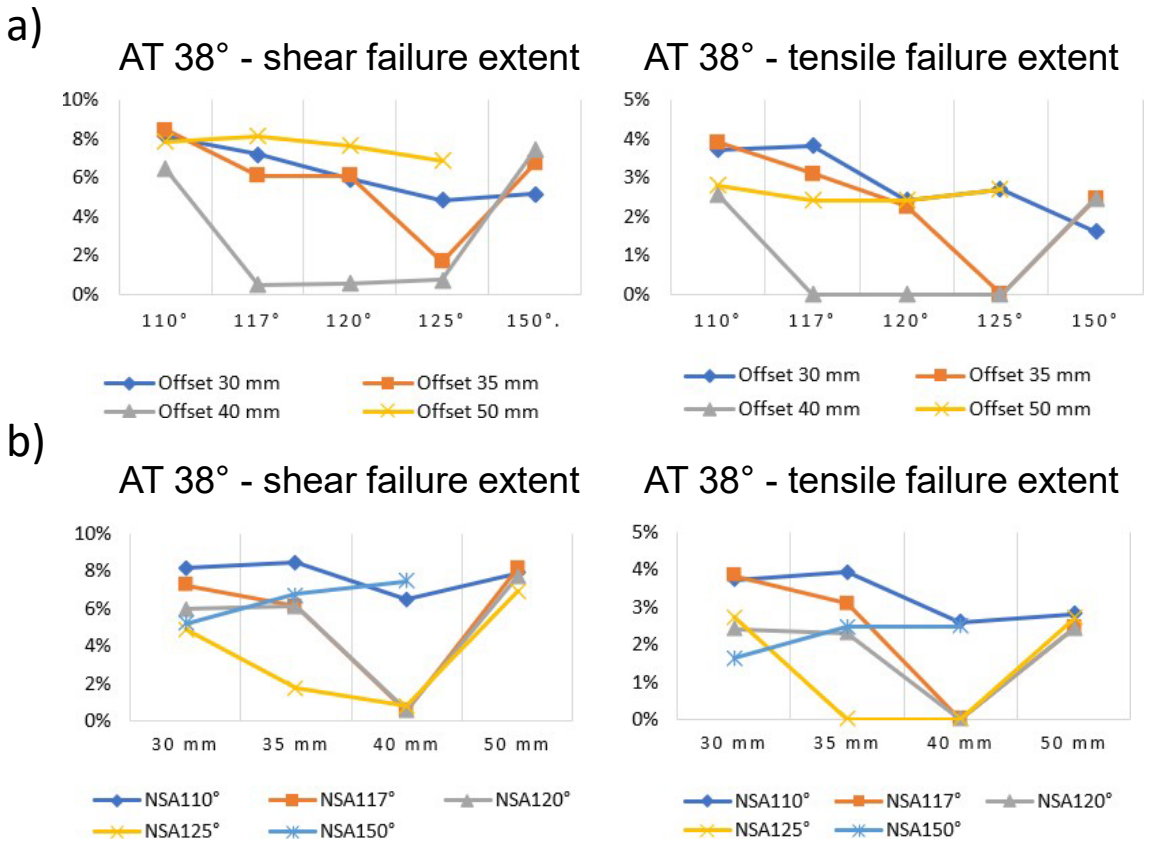

Figure 4: Variations of the shear and tensile stem-cement interface failure extent at AT 38° with (a) offset alterations and (b) NSA alterations

3.2. Stress distribution in the cement mantles

The intercomparison of the stress distributions in the mantles is done following a similar method to the one proposed by Lennon and Prendergast [5], where volume percentages under a specific stress level limit is utilized. A stress level superior 3 MPa is considered critically as it is the limit the cement can withstand 10 million load cycles. In this study, instead of relying on stressed cement volume percentages, the percentages of nodes are used. For all stress limits considered, the percentage points difference between the node percentages determined for both mantles in each model remained inferior to 10%.

Those results show that in all stress limits considered, the variation in AT angles from 8° to 18° does not exert an expressive influence on the node percentages and, therefore, on the stress distributions (see Table 2). However, there is a considerable change in these values with the increase in the AT up to 38°, where the number of nodes with occurring stresses over 3 MPa increases from nearly 0 % (8° and 18° AT) to more than 10 % (38° AT) for both new

and old cement mantle. For constant NSA values, alterations in the femoral offset don't result in strongly linear node percentages variations. The same occurs for variations in the offset or NSAs at constant AT angles.

Table 2: Node percentage mean values for the new and old cement mantles of models with the same AT

	Old Cement Mantle				**New Cement Mantle**			
AT	0-1 MPa	1-2 MPa	2-3 MPa	>3 MPa	0-1 MPa	1-2 MPa	2-3 MPa	>3 MPa
38°	35.57%	28.82%	18.00%	16.79%	39.27%	30.20%	30.17%	11.29%
18°	75.44%	20.59%	2.10%	0.86%	80.31%	17.80%	16.76%	0.00%
8°	79.94%	16.75%	1.69%	0.74%	82.29%	15.77%	14.73%	0.19%

3.3. Contour of stress

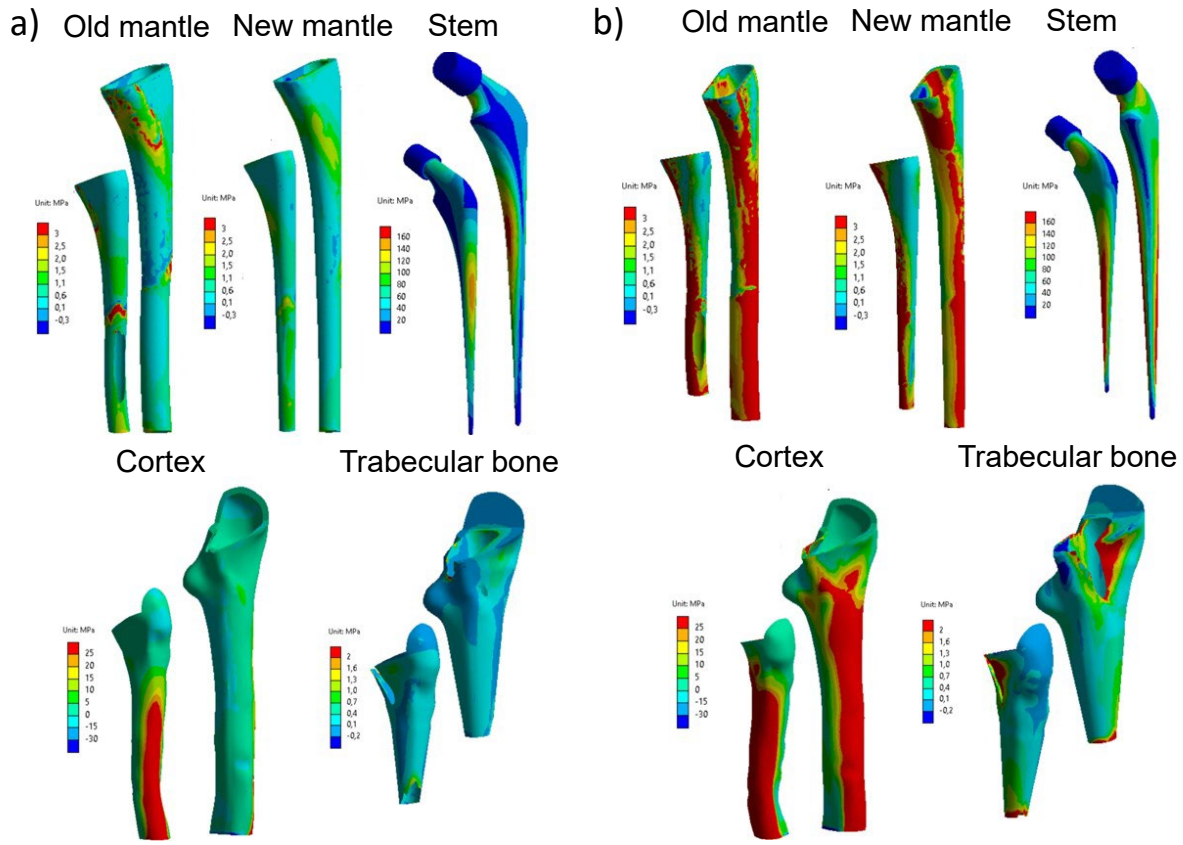

Figure 5: Stress contours given in the implant components of the model at NSA 110° and offset 35 mm and a) AT 18° and b) AT 38°

The stress contours in bone and implant structures show similarity in models with 8° and 18° AT angles (Figure 5a). For these configurations, the highest stresses in the stems are in the middle sections at the lateral and medial regions, and the necks' medial and lateral sides. In prosthetic heads, higher stresses occur at the faces contacting the stems. Old mantles exhibit highest stresses in the proximal region, mainly on the medial side, and on the lateral side in the distal and middle regions. New mantles show highest stresses at the lateral side near the stems' tip and in the middle region, and at the anterior side in the proximal region. The femoral cortex has highest stresses on the lateral side in the middle and distal regions, while the trabecular bone's highest stresses are mostly above the lesser trochanter. The stem-

cement interface has highest shear stresses in the proximal section and highest tensile stresses at the medial side in the proximal region and the lateral side in the middle region.

For models with 38° AT angles, highest stresses in the stems are at the anterior and posterior sides in the middle and distal regions (Figure 5b). The prosthetic heads show higher stresses at the faces contacting the stems. Old mantles have highest stresses at the medial side in the proximal section and the anterior side in the middle and distal regions. New mantles exhibit highest stresses at the anterior and medial sides in the proximal region, and the anterior side in the middle and distal sections. The trabecular bone's highest stresses are above the lesser trochanter, mainly on the posterior and anterior sides, and more distally on the anterior side. The femoral cortex shows higher stresses on the posterior side below the lesser trochanter. For the stem-cement interface, highest shear stresses are in the proximal section, with highest tensile stresses at the posterior side in the proximal region and the anterior and lateral sides.

Peak stress values indicate that tensile maximum principal stresses in the cement mantles exceed the ultimate tensile strength limits (36-47 MPa) for some models with 38° AT, but this affects a small proportion of the cement (less than 2% above 8 MPa). Peak stresses in stems are below 300 MPa, and in femoral heads below 20 MPa. Trabecular bone models have peak stresses below 21 MPa. In cortical geometries with 38° AT, peak tensile stresses exceed average ultimate tensile strengths (51 MPa transverse, 133 MPa longitudinal) but affect a small percentage of nodes, with only 12.1% above 51 MPa and 3.7% above 100 MPa.

4. Discussion

The comparison between the implant designs has shown that the best outcomes happen for all the models with 8° and 18° AT angles, which did not present tensile or shear failure when comparing the stress levels at their interfaces. Additionally, both implant model groups presented the lowest and very similar peak shear and tensile stresses, which did not vary significantly with the alterations in the NSAs and femoral offsets.

However, the same did not occur for the 38° AT models, in which the maximum failed percentage due to shear (8.46%) and tensile stresses (3.92%) occurred for the 110° NSA and 35 mm offset implant. It can be inferred that the non-linearity observed in the node percentages is potentially the result of the differences in the orientation and magnitudes of the hip reaction forces configured in each model under analysis and, therefore, in the manner in which the loads are transmitted to the models. Despite those non-linearities, it is evident that the parameter combinations with the 40 mm offset and/or the 125° NSA resulted in the lowest failed percentages among the models with 38° AT in both failure modalities.

The intercomparison of stress distributions in the mantles could be accurately executed because of the small differences in the total volume of cement around the stem. Their distributions were also found to be less sensitive to the variations in the AT from 8° to 18° when compared with the effects of the increase in any of these values to 38°. These smaller antetorsions resulted in models with the smallest concentrations of stresses above 3 MPa in both new and old cement mantles, with the mean value of node percentages determined for each AT group being inferior to 1%, indicating improved chances of long-term stability when considering the 10 million cycles of stair climbing.

On the other hand, the distributions of stresses above 3 MPa in the models with 38° AT are considerably higher, where the average of the node percentages within this stress range is superior to 11% for the new mantles and 16% in the old mantles. The sudden peak in the tensile stresses of the old and new cement mantles with the increase in the offset from 35 to 40 mm in the model with 8° AT and 117° NSA might have been the result of the insufficient mesh element size in the region where the highest loads were transmitted. However, this result

was not discarded because it still allowed the comparison between the stress distributions through both mantles in the model, and because the node percentages determined for this model are very small while 3 MPa is a stress level with chances of failure slightly superior to zero, not very critical for the long-term stability evaluation conducted in this work.

Furthermore, there is a stronger linearity in the manner the distributions of stresses above 3 MPa take place with variations in the NSAs and femoral offsets in the models with 38.2° AT, where chances of failure have presented the tendency to decrease with the simultaneous increase in the NSA and offset up to 125° and 40 mm, respectively. As for the extent of the stem-cement interface damage, the models presenting at least a 125° NSA or a 40 mm offset have the lowest concentrations of stress levels associated with probabilities of fatigue failure.

Additionally, in terms of the comparison of the stress distributions between the mantles contained in each model, it was noticeable that the stresses in these structures are very similarly distributed, with the percentage points difference between the node percentages determined for both mantles being inferior to 10%. This proximity in the stress distributions might be explained by the geometrical similarity between mantles and their close load-bearing capacity due to the proximity in the Young's Modulus attributed to the old-cement mantle (2.08 GPa) and the new-cement mantle (2.12 GPa).

5. Conclusion

The selection of an optimum combination of hip parameters for the muscle function of a patient after revision THA can be done with simulations of ADL using patient-specific MSM that is scaled into the patient's bone geometries. However, for a more complete comprehension of the operative outcomes, it is important to inspect the stress distributions in the implant components. For this matter, preclinical tests based on FE analysis can be conducted where FE models are configured with the load data from the ADL simulation results and femur bone CAD geometries obtained from MRI images.

The present work was, therefore, an example of how FE models can be used to analyse the influence that hip parameters have on the stress distributions in the bone-implant interface. The method for estimating the long-term stability of the cemented stem fixation after cement-in-cement revision of the stem in THA allows a fast comparison of the stress distributions between different FE models and made evident that AT, NSAs, and femoral offsets have the potential to influence the chances of stem-cement and cement bulk failure. However, the most expressive change in the stress distributions is observed for the increase in the AT. Thus, the results of this work in combination with the results of Scherb et al. [9] show that a comprehensive approach integrating musculoskeletal simulation and FE simulation can help the clinicians to design a revision hip implant optimally suited for a certain patient, both incorporating the long-term stability of the implant and the load on the weakened muscles.

References

[1] Grimberg, A. ; Jansson, V. ; Lützner, J. ; Melsheimer, O. ; Morlock, M. ; Steinbrück, A.: EPRD-Jahresbericht 2020. Berlin : EPRD Deutsche Endoprothesenregister, 2020

[2] Rupp, M. ; Lau, E. ; Kurtz, S. M. ; Alt, V.: Projections of Primary TKA and THA in Germany From 2016 Through 2040. In: *Clinical orthopaedics and related research* 478 (2020), Nr. 7, S. 1622–1633

[3] Stolk, J. ; Verdonschot, N. ; Cristofolini, L. ; Toni, A. ; Huiskes, R.: Finite element and experimental models of cemented hip joint reconstructions can produce similar bone and cement strains in pre-clinical tests. In: *Journal of biomechanics* 35 (2002), Nr. 4, S. 499–510

[4] Stolk, J. ; Maher, S. A. ; Verdonschot, N. ; Prendergast, P. J. ; Huiskes, R.: Can finite element models detect clinically inferior cemented hip implants? In: *Clinical orthopaedics and related research* (2003), Nr. 409, S. 138–150

[5] Lennon, A. B. ; Prendergast, P. J.: Evaluation of cement stresses in finite element analyses of cemented orthopaedic implants. In: *Journal of biomechanical engineering* 123 (2001), Nr. 6, S. 623–628

[6] Hung, J.-P. ; Bai, Y.-W. ; Hung, C.-Q. ; Lee, T.-E.: Biomechanical Performance of the Cemented Hip Stem with Different Surface Finish. In: *Applied Sciences* 9 (2019), Nr. 19, S. 4082

[7] Madsen, M. S. ; Ritter, M. A. ; Morris, H. H. ; Meding, J. B. ; Berend, M. E. ; Faris, P. M. ; Vardaxis, V. G.: The effect of total hip arthroplasty surgical approach on gait. In: *Journal of orthopaedic research : official publication of the Orthopaedic Research Society* 22 (2004), Nr. 1, S. 44–50

[8] Pfirrmann, C. W. A. ; Notzli, H. P. ; Dora, C. ; Hodler, J. ; Zanetti, M.: Abductor tendons and muscles assessed at MR imaging after total hip arthroplasty in asymptomatic and symptomatic patients. In: *Radiology* 235 (2005), Nr. 3, S. 969–976

[9] Scherb, D. ; Fleischmann, C. ; Sesselmann, S. ; Miehling, J. ; Wartzack, S.: Evidence for the Applicability of Musculoskeletal Human Models to Improve Outcomes of Total Hip Arthroplasty, Bd. 38. In: Tavares, João Manuel R. S.; Bourauel, Christoph; Geris, Liesbet; Vander Slote, Jos (Hrsg.): *Computer Methods, Imaging and Visualization in Biomechanics and Biomedical Engineering II*. Cham : Springer International Publishing, 2023 (Lecture Notes in Computational Vision and Biomechanics), S. 194–207

[10] Kebbach, M. ; Hucke, L. ; Kluess, D. ; Miehling, J. ; Scherb, D. ; Wartzack, S. ; Wechsler, I. ; Wittek, A. ; Woiczinski, M. ; Schwarze, M.: Numerische Simulation in der muskuloskelettalen Biomechanik : Anwendungsperspektiven und Möglichkeiten. In: *Orthopadie (Heidelberg, Germany)* (2024)

[11] Cnudde, P. H. J. ; Kärrholm, J. ; Rolfson, O. ; Timperley, A. J. ; Mohaddes, M.: Cement-in-cement revision of the femoral stem: analysis of 1179 first-time revisions in the Swedish Hip Arthroplasty Register. In: *The bone & joint journal* 99-B (2017), 4 Supple B, S. 27–32

[12] Lieberman, J. R. ; Moeckel, B. H. ; Evans, B. G. ; Salvati, E. A. ; Ranawat, C. S.: Cement-within-cement revision hip arthroplasty. In: *The Journal of bone and joint surgery. British volume* 75 (1993), Nr. 6, S. 869–871

[13] Quinlan, J. F. ; O'Shea, K. ; Doyle, F. ; Brady, O. H.: In-cement technique for revision hip arthroplasty. In: *The Journal of bone and joint surgery. British volume* 88 (2006), Nr. 6, S. 730–733

[14] Fleischmann, C. ; Scherb, D. ; Leher, I. ; Wolf, A. ; Miehling, J. ; Wartzack, S. ; Sesselmann, S.: Segmentation of Musculotendinous Structures of the Hip from 3D Imaging for Patient-Specific Individualization of Biomechanical Simulations, Bd. 1253. In: Ahram, Tareq; Taiar, Redha; Langlois, Karine; Choplin, Arnaud (Hrsg.): *Human Interaction, Emerging Technologies and Future Applications III*. Cham : Springer International Publishing, 2021 (Advances in Intelligent Systems and Computing), S. 331–337

[15] Dorr, L. D. ; Faugere, M. C. ; Mackel, A. M. ; Gruen, T. A. ; Bognar, B. ; Malluche, H. H.: Structural and cellular assessment of bone quality of proximal femur. In: *Bone* 14 (1993), Nr. 3, S. 231–242

[16] Ebramzadeh, E. ; Sarmiento, A. ; McKellop, H. A. ; Llinas, A. ; Gogan, W.: The cement mantle in total hip arthroplasty. Analysis of long-term radiographic results. In: *The Journal of bone and joint surgery. American volume* 76 (1994), Nr. 1, S. 77–87

[17] Berg, A. J. ; Hoyle, A. ; Yates, E. ; Chougle, A. ; Mohan, R.: Cement-in-cement revision with the Exeter Short Revision Stem: A review of 50 consecutive hips. In: *Journal of clinical orthopaedics and trauma* 11 (2020), Nr. 1, S. 47–55

[18] Woodbridge, A. B. ; Hubble, M. J. ; Whitehouse, S. L. ; Wilson, M. J. ; Howell, J. R. ; Timperley, A. J.: The Exeter Short Revision Stem for Cement-in-Cement Femoral Revision: A Five to Twelve Year Review. In: *The Journal of arthroplasty* 34 (2019), 7S, S297-S301

[19] Kluess, D. ; Bergschmidt, P. ; Mittelmeier, W. ; Bader, R.: Ceramics for joint replacement. In: *Joint Replacement Technology* : Elsevier, 2014, S. 152–166

[20] Knauss, P.: Materialkennwerte und Festigkeitsverhalten des kompakten Knochengewebes an coxalen Human-Femur. In: *Biomedizinische Technik. Biomedical engineering* 26 (1981), Nr. 12, S. 311–315

[21] Knauss, P.: Materialkennwerte und Festigkeitsverhalten des spongiösen Knochengewebes am coxalen Human-Femur. In: *Biomedizinische Technik. Biomedical engineering* 26 (1981), Nr. 9, S. 200–210

[22] Reilly, D. T. ; Burstein, A. H.: The elastic and ultimate properties of compact bone tissue. In: *Journal of biomechanics* 8 (1975), Nr. 6, S. 393–405

[23] Delp, S. L. ; Anderson, F. C. ; Arnold, A. S. ; Loan, P. ; Habib, A. ; John, C. T. ; Guendelman, E. ; Thelen, D. G.: OpenSim: open-source software to create and analyze dynamic simulations of movement. In: *IEEE transactions on bio-medical engineering* 54 (2007), Nr. 11, S. 1940–1950

[24] Leher, I. ; Fleischmann, C. ; Scherb, D. ; Kollerer, M. ; Miehling, J. ; Wartzack, S. ; Sesselmann, S.: Patient-Specific Modelling for Preoperative Estimation of Hip Mechanics for Improved Planning of Total Hip Endoprosthesis Using Multibody Simulations, Bd. 319. In: Ahram, Tareq; Taiar, Redha (Hrsg.): *Human Interaction, Emerging Technologies and Future Systems V*. Cham : Springer International Publishing, 2022 (Lecture Notes in Networks and Systems), S. 1088–1096